Atmospheric Environment 242 (2020) 117835

Contents lists available at ScienceDirect

Atmospheric Environment

journal homepage: http://www.elsevier.com/locate/atmosenv

Observations of new particle formation, modal growth rates, and direct emissions of sub-10 nm particles in an urban environment

Alyssa Zimmerman [a], Markus D. Petters [a,*], Nicholas Meskhidze [a]

[a] Department of Marine, Earth, and Atmospheric Sciences, North Carolina State University, Raleigh, NC, USA

HIGHLIGHTS

- A monthly average of 8 new particle formation events contribute to the ultrafine particle number concentration.
- Multiple distinct anthropogenic sources of sub-10 nm sized particles are identified.
- A slight reduction in number concentration was observed during the the COVID-19 pandemic.

ARTICLE INFO

Keywords:
Urban aerosol
New particle formation
Sub-10 nm aerosol
Air pollution

ABSTRACT

Ultrafine particles with diameters less than 100 nm suspended in the air are a topic of interest in air quality and climate sciences. Sub-10 nm particles are of additional interest due to their health effects and contribution to particle growth processes. Ambient measurements were carried out at North Carolina State University in Raleigh, NC between April to June 2019 and November 2019 to May 2020 to investigate the temporal variability of size distribution and number concentration of ultrafine particles. A mobile lab was deployed between March and May 2020 to characterize the spatial distribution of sub-10 nm particle number concentration. New particle formation and growth events were observed regularly. Also observed were direct emissions of sub-10 nm particles. Analysis against meteorological variables, gas-phase species, and particle concentrations show that the sub-10nm particles dominated number concentration during periods of low planetary boundary layer height, low solar radiation, and northeast winds. The spatial patterns observed during mobile deployments suggest that multiple temporally stable and spatially confined point sources of sub-10 nm particles are present within the city. These sources likely include the campus utility plants and the Raleigh-Durham International Airport. Additionally, the timing of data collection allowed for investigation of variations in the urban aerosol number size distribution due to reduced economic activity during the COVID-19 pandemic.

1. Introduction

Urban environments experience some of the largest aerosol number concentrations resulting from anthropogenic emissions. Many of these particles are within the ultrafine particle (UFP) range, which are particles having diameters less than 100 nm. Ultrafine particles contribute to aerosol radiative forcing directly through the scattering and absorption of sunlight, and indirectly through changes in cloud microphysical properties (Myhre et al., 2013). Long term exposure to UFPs negatively affects cardiovascular and respiratory health in humans (Li et al., 2003; Wichmann and Peters, 2000). Particle deposition models show that most UFPs reach the pulmonary region of the lungs which exacerbates pre-existing respiratory illnesses (Asgharian and Price, 2007; Peters et al., 1997). Particles with diameters <25 nm in diameter (nucleation mode) (Agus et al., 2008; Willis et al., 2016; D. Yue et al., 2009) are particularly harmful. Because of their small size, the particles deposit higher within the respiratory system in the nasopharyngeal and tracheobronchial regions. Within these regions, the particles cross the mucous membrane and circumvent the blood-brain barrier into the central nervous system causing disruption and potential death of nerve cells (Alföldy et al., 2009; Asgharian and Price, 2007; Oberdörster et al., 2004). Additionally, nucleation mode particles are cytotoxic to our skin cells and can lead to the demise of healthy cells (Malorni et al., 2017).

Atmospheric new particle formation (NPF) plays an important role in

* Corresponding author. NC State University, Department of Marine, Earth and Atmospheric Sciences, Campus Box 8208, Raleigh, NC, 27695, USA.
E-mail addresses: mdpetter@ncsu.edu (M.D. Petters), nmeskhi@ncsu.edu (N. Meskhidze).

https://doi.org/10.1016/j.atmosenv.2020.117835
Received 26 June 2020; Received in revised form 29 July 2020; Accepted 31 July 2020
Available online 7 August 2020

the atmospheric aerosol number budget, with influences on cloud formation and climate (Seinfeld and Pandis, 2006). Volatile compounds, either from natural or anthropogenic sources are oxidized in the atmosphere and form lower volatile species. These can spontaneously form clusters <3 nm in size. Under some circumstances, the pool of clusters "activate" and form large concentrations of particles that subsequently grow to 20–100 nm in size by coagulation and additional vapor condensation (M. Kulmala, 2003; Zhang and Wexler, 2002). Nucleation and modal growth of particles is primarily characterized as episodic and is referred to as an NPF event (Dal Maso et al., 2005). NPF events are observed in urban, rural, and remote locations worldwide (Kerminen et al., 2018; Nieminen et al., 2018). Multi-location measurements suggest that NPF events occur both locally, and regionally exceeding hundreds of kilometers (Bousiotis et al., 2019; Kerminen et al., 2018; Kalkavouras et al., 2020; Németh et al., 2018; Wehner et al., 2007; Yue et al., 2013). The atmospheric condensation sink, which is dependent on the pre-existing aerosol concentration, plays a key role in the occurrence of NPF events (Dal Maso, 2002). By acting as a sink for volatile compounds and small clusters, a high pre-existing aerosol load can hinder NPF (Hussein et al., 2020; Salma et al., 2016; Z. B. Wang et al., 2013). The frequency, strength, and particle growth rates of NPF events also vary greatly with local meteorology. High solar radiation and low relative humidity positively correlate with the occurrence of NPF events (Baranizadeh et al., 2014; Boy and Kulmala, 2002; Jaatinen et al., 2009; Pryor et al., 2011). These conditions promote the photochemical production of nucleating or condensable species that contribute to NPF (Harrison et al., 2000; O'Dowd et al., 1999). Nucleation events also occur both at the surface and aloft in the atmosphere. High-altitude measurements on mountain-tops (Bianchi et al., 2016; Rose et al., 2015) and through aircrafts (Mirme et al., 2010; Schröder and Ström, 1997) suggests that nucleation can occur in the free troposphere. Nucleation can also occur in a residual layer in the remnants of the previous day's mixed layer. Diurnal variations in the planetary boundary layer height (PBLH) influence the detection of the residual layer NPF events at the surface. Turbulent mixing during the growth of the daytime convective boundary layer leads to downward mixing of particles that were nucleated aloft in the residual layer. The nucleated particles grow slightly before they are detected at the surface and grow further resulting in an NPF event (Größ et al., 2018; Meskhidze et al., 2019; Nilsson et al., 2001; Platis et al., 2016; Stanier et al., 2004; Stratmann et al., 2003).

NPF events are classified using various methods based on the strength, continuity, and size of nucleated particles (Boy and Kulmala, 2002; Dal Maso et al., 2005; Németh et al., 2018). One specific classification scheme categorizes the events based on the initial size and the growth to larger sizes of nucleated particles as Class A, B or C (Boy and Kulmala, 2002; Mäkelä et al., 2000; Pillai et al., 2013; Pryor et al., 2010). Class A events are defined by the detection of 3 nm sized particles in an initial nucleation mode that grows continually to larger sizes (Boy and Kulmala, 2002). The nucleated particles in Class B events also undergo persistent modal growth; however, the nucleated particles are either less clear than the previous class (Boy and Kulmala, 2002; Mäkelä et al., 2000) or new particles are not observed below 10 nm (Pillai et al., 2013), or 25 nm (Pryor et al., 2010). Finally, an event is classified as Class C if an increase in UFP number concentration resulting from nucleation occurs, but no continuous modal growth follows (Boy and Kulmala, 2002; Mäkelä et al., 2000; Pillai et al., 2013; Pryor et al., 2010). Class C events are also referred to as 'Undefined' in some cases (Boy et al., 2008).

UFPs in urban environments can also be emitted directly from a multitude of sources. The mean diameter of particles released from traditional gasoline vehicles ranges between 7 and 20 nm (Cheung et al., 2011; Morawska et al., 2008) and often makes up a significant fraction of the nucleation mode particle number concentration (Karl et al., 2016). The contribution of UFPs to the urban particle number concentration is prominently visible during rush hour traffic (Meskhidze et al., 2019). Ambient measurements near airports in California (Hudda et al., 2014; Zhu et al., 2011); China (Ren et al., 2016); Cyprus (Brilke et al., 2020); and the Netherlands (Keuken et al., 2012) measured nucleation mode particle concentrations greater than 1×10^5 cm^{-3}. The mode diameter of the airport size distributions range between 11 and 16 nm, meaning nearly half of the distribution is less than 10 nm in diameter (Brilke et al., 2020; Ren et al., 2016; Zhu et al., 2011). Natural gas burning combustion plants also emit a significant number of particles between 2 and 7 nm (Brewer et al., 2016; Shi et al., 2001). The mean diameter of particles emitted by power plants is approximately 5 nm and increases with decreasing energy load (Bond et al., 2006). Natural gas also produces 2–5 nm particle number concentrations greater than 1×10^6 cm^{-3} when burned in passenger car engines (Alanen et al., 2015), or used in home and water heating appliances (Minutolo et al., 2008). Urban studies have also inadvertently measured the continuous emission of nucleation mode particles resulting from local combustion sources such as power plants (Gao et al., 2009), airports (Cheung et al., 2011), and funeral homes (D. Wang et al., 2014). Measurements of the pollutant plumes from these sources demonstrate a steady presence of sub-10 nm particles. No modal growth of these particles is measured suggesting that the aerosols resulted from a local direct emissions as opposed to a regional-scale NPF event (Cheung et al., 2011; Gao et al., 2009; D. Wang et al., 2014). An increase in the nucleation mode particle number concentration that persists for multiple hours without the occurrence of modal growth is referred to as a nucleation burst or particle burst (PB) event. A continual geometric mean diameter ranging from 8 to 32 nm is maintained throughout the duration of an event (Cheung et al., 2011; D. Wang et al., 2014). Spikes in the nucleation mode aerosol number concentration during PB events often exceed values of 1×10^5 cm^{-3} (Gao et al., 2009). The events correlate with periods of low solar radiation, low temperatures, and high relative humidity; resulting in weaker aerosol dispersion processes. Therefore, it is believed that the detection of PB events is largely due to the continuous emission of particles from local sources during calm atmospheric conditions (D. Wang et al., 2014).

The importance of Class A, B, and C NPF events has been explored in Duke Forest located ~39 km NW of Raleigh, NC by Pillai et al. (2013). The impacts of boundary layer evolution and local traffic emissions on the urban aerosol size distribution in Raleigh, NC have been previously investigated by Meskhidze et al. (2019). However, little is known about the multitude of local point sources emitting sub-40 nm particles which are likely affecting the urban aerosol number size distribution in the Southeastern U.S.

This work presents analysis of aerosol size distribution data collected from April 2019 to June 2019 and November 2019 to May 2020 from two stationary ambient aerosol measurement campaigns in Raleigh, NC and a mobile measurement system, deployed between March and May 2020. The aerosol size distribution data was analyzed for frequency and strength of NPF and PB events. Local meteorological and gaseous pollutant data allow for analysis of favorable event conditions. The mobile system measured the spatial distribution of sub-10 nm particles providing insight on potential particle sources throughout the Raleigh metro area. Finally, the timing of this study allows for investigation of changes in the urban aerosol size distribution due to reduced economic activity during the COVID-19 outbreak.

2. Methods

2.1. Site description

Ambient aerosol measurements were performed at Jordan Hall, located on North Carolina State University's (NCSU) Campus (35°46′53.59″N, 78°40′33.03″W). The measurement site was located 3.2 km west of downtown Raleigh (Fig. S1). Western Blvd., one of the arteries that connect the suburbs with downtown Raleigh, is adjacent to the building. According to volume reports from the NC Department of

Transportation (NCDOT, http://ncdot.maps.arcgis.com), the average daily weekday traffic on Western Blvd. is more than 30,000 vehicles per day. Heavy morning (07:00–09:00) and evening (16:00–18:00) rush hour traffic persists throughout the week with more than 2500 vehicles per hour. Vehicle traffic is even greater along the Interstate Beltline. The closest segment of Interstate 440 (inner-loop of Beltline) is located 2 km west of the NCSU campus and NCDOT recorded an annual average daily total of 116,000 vehicles per day in 2018. Interstate 540 (outer-loop of Beltline) is ~17 km NW of campus and the annual average daily total in 2018 was 98,000 vehicles per day (NCDOT).

The Raleigh-Durham International Airport (RDU; 17 km NW of campus) and local campus utility plants also contribute to local anthropogenic emissions. On the NCSU main campus is the Cates Ave. Utility Plant and Yarbrough Dr. Boiler, located 0.3 km NNE and 0.9 km NE of Jordan Hall, respectively (Fig. S2). The Cates Ave. Plant is a co-generation plant using natural gas that provides energy to the central and north campuses. A second utility plant, the Centennial Campus Utility Plant is located 0.7 km to the SSE of Jordan Hall. This plant generates chilled water and steam for the buildings on NCSU's centennial campus.

To investigate the spatial and temporal variability of aerosols in Raleigh, three different instrumentation configurations, detailed in Table 1, were used during measurements taken from April 19 to June 4, 2019 and again from November 15, 2019 to May 15, 2020. Instrumentation for aerosol size distribution and number concentration measurements were situated on the rooftop of Jordan Hall (~23 m above ground level) for the spring 2019 measurements. From November 15, 2019 to May 15, 2020 the size distribution and number concentration instruments were moved into a fourth-floor laboratory on the north side of the building, ~20 m above ground level. The instruments were operated in the laboratory, as opposed to the rooftop, to allow for easier accessibility. The inlet for these instruments sampled ambient air from a sampling line protruding 15 cm away from the building through a partially opened window. Finally, from March to May 2020, a mobile deployment system was constructed to further investigate the spatial distribution of sub-10 nm particles throughout Raleigh. This system consisted of instrumentation for aerosol number concentration measurements and continually sampled from the Jordan Hall laboratory, until it was transported to a vehicle for mobile deployments.

2.2. Size distribution and number concentration measurements

During the spring 2019 measurement campaign, ambient aerosol size distribution and number concentration measurements were performed using a scanning mobility particle sizer (SMPS) and condensation particle counter (CPC). The SMPS consisted of a radial differential mobility analyzer (RDMA) and CPC (CPC-1, TSI Inc. 3020) measuring diameters greater than 5 nm. The RDMA system was configured with sheath-to-sample flow ratio of 6:1.5 L min^{-1}. The RDMA scanned from a mobility diameter range of 80 to 5 nm; however, after inversion, the upper limit was cropped to 55 nm. Cropping was necessary because no upstream aerosol impactor was available, which leads to inversion errors in the 55–80 nm size range. The RDMA SMPS system was deployed again during the fall/spring 2019/2020 campaign, but with a different CPC (CPC-2, TSI Inc. 3022A).

Table 1
Measurement dates, location, instrumentation and size range of particles measured.

Measurement Dates	Location	Instrumentation	Measured Size Range
Apr. 19 – June 4, 2019	Rooftop of Jordan Hall	SMPS (RDMA) & CPC-1 (TSI Inc. 3020)	5–55 nm
Nov. 15 – May 15, 2020	4th Floor Lab in Jordan Hall	SMPS (RDMA) & CPC-2 (TSI Inc. 3022A)	5–55 nm
Mar.–May 2020	4th Floor Lab and Vehicle	CPC-3 (TSI Inc. 3776c)	>2.5 nm
		CPC-4 (TSI Inc. 3762) until May 4	>11 nm
		CPC-5 (TSI Inc. 3772) May 9–15	>10 nm

The mobile deployment system used in spring 2020 consisted of two CPCs (CPC-3, TSI 3776c; and CPC-4, TSI 3762) detecting diameters greater than 2.5 nm and 11 nm, respectively (manufacturer specification). Data were recorded at 10 Hz frequency sampling the digital pulse output and 1 Hz frequency using serial acquisition. While in the laboratory, the twin CPC system sampled parallel to the SMPS and was removed temporarily for mobile sampling. CPC-4 sampled the air using pulse counts. Pulse counts were coincidence corrected using the method described in Collins et al. (2013). The coincidence correction was calculated using a sample flow rate of 50 cm^3 s^{-1} and an average beam residence time of 2×10^{-5} s (manufacturer specification). For the CPC-4 model, the flow rate was controlled using a critical orifice. The built-in signal processing was used for CPC-3. The sample flow rate was continuously measured and coincidence was corrected through live-time counting performed by the manufacturer's algorithm. This method divides the number of counted particles by the time between electrical pulses and the flow rate to provide an accurately determined true counting rate. Due to instrumentation failure, CPC-4 was replaced with CPC-5 (TSI 3772) in May 2020. The difference in the counts between CPC-3 and CPC-4/5 provided a particle number concentration for diameters between 2.5 and 11 nm ($N_{2.5–11nm}$, 10 nm upper limit when CPC-5 was used). CPC-5 was used during mobile deployments 5 and 6.

2.3. SMPS inversion

All raw 10 Hz data from the SMPS system and corresponding CPC were inverted using the method described in Petters (2018). The inversion method includes mapping the time varying electric field to a corresponding mobility diameter (S. C. Wang and Flagan, 1990). Particle counts are binned and inverted to the total concentration by accounting for the SMPS transfer function, multiple charges, and diffusional broadening of the transfer function. The resulting concentration and particle diameter data from the SMPS were binned into 83 logarithmically spaced bins spanning a size range of 5–55 nm. The binned SMPS data was then averaged onto fixed 5 min and 30 min time grids to facilitate time-series analysis.

Fig. 1 presents the temporal variability in the 5–55 nm spectral number density during January 2020 based on the 30 min averaged dataset (The entire timeseries from both stationary deployments is available in Figs. S3 and S4). NPF and PB events occurred during nearly all months of measurement and contribute significantly to the nucleation mode number concentration in Raleigh, NC. In January, there were four Class A NPF events (5th, 6th, 8th, and 28th), and three Class B events (6th, 8th, and 28th). Additionally, a short PB event occurred between midnight and 17:30 on the 17th; and a lengthy event beginning at 09:00 on the 20th and lasting through 06:00 on the 24th.

2.4. NPF and particle burst event classification

The aerosol size distribution data from each day of the measurement campaigns was visually inspected to determine whether there was an NPF or PB event. NPF event days were characterized by the appearance of nucleation mode particles leading to increased aerosol number concentration, followed by continuous modal growth (Dal Maso et al., 2005). Visual analysis of normalized spectral number density plots was used to categorize NPF events into Classes A, B, or C based on criteria previously established in literature (Boy and Kulmala, 2002; Pillai et al., 2013; Pryor et al., 2010). NPF events were classified as Class A when the initial nucleation mode particles were present at 5 nm and grew into the Aitken mode. Class B events had an initial mode between 10 and 20 nm and the particles also grew to larger sizes. Finally, if there were nucleation mode particles present, resulting in an increase in the ultrafine

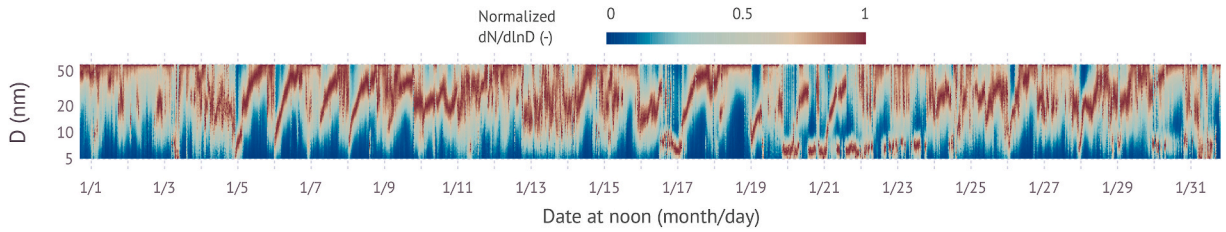

Fig. 1. Normalized spectral number density from the SMPS for January 2020.

particle number concentration, but growth was not continuous or sustained, this event was classified as Class C. More specifically Class C events were characterized by modal growth lasting <4 h, or significant modal shrinkage of particles. Examples of Class A, B, and C NPF events are shown in Figs. S5, S6, and S7. The dates and times of all Class A and B NPF events are detailed in Tables S1 and S2. A slide deck analyzing the normalized spectral number density of all observed nucleation events is included in the archived dataset.

Visual analysis of the size distribution data also revealed the presence of PB events. These events were characterized by continuous bursts of nucleation mode particles that persisted for multiple hours or days while maintaining a constant geometric mean diameter (Cheung et al., 2011; D. Wang et al., 2014). Events were classified as a PB event, as opposed to a Class C NPF event, if multiple bursts of nucleation mode particles continued for more than 6 h and no modal growth was observed. The 30-min average of 5–10 nm particles was visually analyzed for each PB event to estimate a threshold concentration that was exceeded by each burst in an event. Due to variations in strength of events and background number concentration, each event was assigned a separate threshold concentration (shown in Table S3). The threshold concentrations were determined by the maximum 30-min average number concentration of the weakest particle burst during each event. The threshold values were then used to estimate the PB event duration. The start and end times of each event were estimated as when the 30-min average 5–10 nm number concertation surpassed and receded the threshold concertation.

2.5. Growth rate calculation

The growth rates were calculated for Class A and B NPF events using the maximum concentration method of Kulmala et al. (2012). The detection time of each event was initially estimated from visual inspection of normalized number spectral density plots. For each scan during the event, the modal diameter was calculated from the maximum number concentration and then plotted as a function of time. The growth rates of each event were derived using a linear regression of the modal diameters across three size ranges of 5–10 nm, 10–20 nm, and 20–30 nm. The first size range was selected based on the lower limit of the SMPS instrument. Considering that the initial mode diameter of Class B events was approximately 10 nm, the second size range captures the initial growth of nucleated particles during these events. The second and the third size ranges allow for comparison of growth rates between the Class A and B events. Due to the 5 nm lower limit in the size distribution data, the growth rates calculated between 5 and 10 nm were used to estimate the approximate start time of each Class A event. However, growth rates below 10 nm vary greatly with size. Yli Juuti et al. (2011) reported average growth rates between 1.5 and 3 nm are nearly half of the growth rates measured above 3 nm. Considering this variability in growth rates below 10 nm, the Class A event start times are reported within a possible range based on one standard deviation of the 5–10 nm growth rates. Class B start times are reported as a single time, rather than a range, because the initial mode detected was greater than the lower limit of the SMPS and the initial appearance of these particles can be accurately estimated.

2.6. Mobile deployments

To investigate potential sub-10 nm particle sources, the mobile system was deployed 6 times between March and May 2020. During mobile sampling, the inlet for the particle counters was placed out the rear passenger side window. A 1000-Watt lithium battery power station was used to operate the CPCs, which provided approximately 3.5 h of sample time. Time series of the driving route coordinates were recorded using a mobile phone application. The particle counts were then averaged on a time grid, ranging between 6 and 7.5 s depending on the mobile deployment, to match the coordinate dataset. Details of the individual deployments are shown in Table 2. Two different routes were driven during the various deployments. The first, shown in Figs. S8 and S9 was designed to maximize distance traveled around Raleigh and highlight any concentration gradient present between downtown and the suburbs. This route was used in mobile deployments 1–3. The second route (Figs. S10 and S11) was designed locally around the NCSU campus and was used in mobile deployments 4–6.

2.7. Meteorological, gaseous pollutant, and traffic data

One-minute data for temperature, pressure, wind speed and direction, precipitation, and solar radiation were acquired from the North Carolina Climate Office weather station located on the rooftop of Jordan Hall. Hourly PBLH data were obtained from the North American Mesoscale Forecast System (NAM) at a 12 km spatial resolution. Hourly data for CO, NO_2, O_3, $PM_{2.5}$, and PM_{10} were acquired from the Environmental Protection Agency's (EPA) AQS API system for the Millbrook School site (AQS ID: 37-183-0014). The Millbrook School site is in the Northeast suburbs of downtown Raleigh and is 12.4 km NE of the sampling site. Hourly gaseous pollutant data for SO_2 was unavailable at any nearby monitors, and therefore was not analyzed. Daily traffic volume reports for Western Blvd. (Location ID: 0920000006) were retrieved from the North Carolina Department of Transportation. Human movement data was retrieved from Google's COVID-19 Community Mobility Report for Wake County, NC.

3. Results and discussion

3.1. Temporal evolution

Fig. 2 shows the daily average number concentration time series from all available instruments. The average integrated SMPS number concentration between 5 and 10 nm ($N_{5–10nm}$), and 10–40 nm ($N_{10–40nm}$) were 1.6×10^3 cm^{-3} and 4.3×10^3 cm^{-3}. These values show that on average, $N_{5–10nm}$ accounts for ~27% of less than 40 nm sized particle number concentration. For periods where the SMPS and dual CPC system was available, there are concurrent time series number concentrations. For example, N > 11 nm and $N_{10–40nm}$ correlate. The daily average number concentrations >2.5, and >11/10 nm from CPCs 3 and 4/5 were 5.3×10^3 cm^{-3} and 1.1×10^4 cm^{-3}, respectively. The average $N_{2.5–11nm}$ computed from the difference in the two CPCs was 5.7×10^3 cm^{-3} which is greater than the $N_{5–10nm}$ measured by the SMPS. The average $N_{5–10nm}$ and $N_{10–40nm}$ during the spring 2019 campaign were nearly half of the average concentrations measured during November and

Table 2
Details of the mobile deployments performed in 2020.

MD	Date	Start Time	End Time	Distance Traveled (km)	Avg. $N_{2.5–11nm}$ (cm^{-3})[a]	Avg. Temperature (°C)	Avg. Wind Direction (degrees)
1	Mar. 4, 2020	13:59	17:30	157	3.7×10^4	15.0	210.4 (SSW)
2	Mar. 19, 2020	11:12	13:58	157	2.3×10^4	22.7	230.6 (SW)
3	Mar. 23, 2020	08:48	11:19	150	3.4×10^4	7.6	207.4 (SSW)
4	Apr. 29, 2020	08:23	09:14	27	4.3×10^3	20.7	219.9 (SW)
5	May 11, 2020	08:20	09:15	26	5.9×10^3	15.4	283.9 (WNW)
6	May 15, 2020	08:05	08:41	19	1.1×10^4	20.7	226.3 (SW)

[a] The average number concentration reported for mobile deployments 5 and 6 is between 2.5 and 10 nm as CPC-5 was used during this deployment.

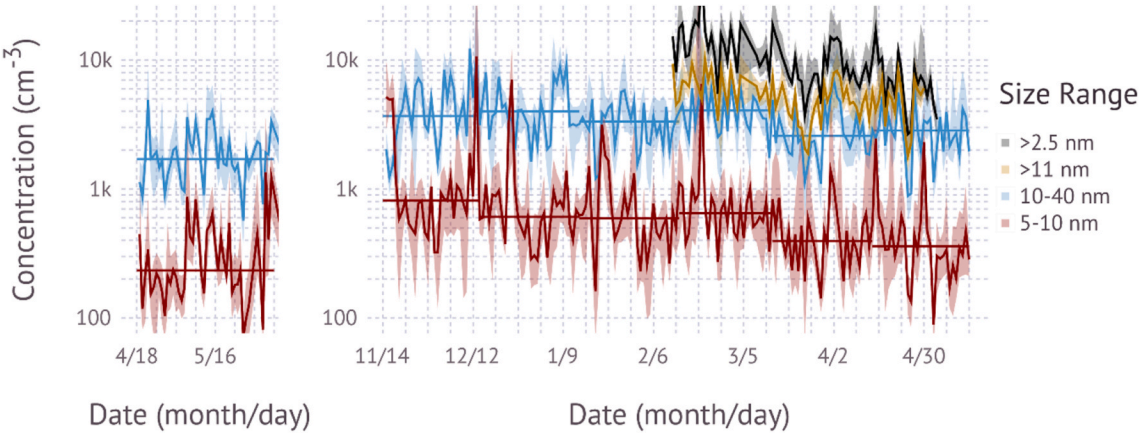

Fig. 2. Daily average integrated SMPS concentration for 5–10 nm (red) and 10–40 nm (blue) size range, number concentration greater than 2.5 nm (black) and greater than 11/10 nm (gold). Vertical ticks are spaced one week apart. Horizontal lines show monthly averages for 5–10 and 10–40 nm particles. (For interpretation of the references to colour in this figure legend, the reader is referred to the Web version of this article.)

December 2019. The number concentrations began to drop again during spring 2020 possibly due to reduced economic activity during COVID-19 (see below). However, the decrease in concentration may also be due to an intra-annual variability, as the concentrations dropped to values nearing those recorded in spring 2019. The observed average $N_{5–10nm}$ was slightly less than the 5.5–10 nm concentration measured in Hong Kong, China (2.5×10^3 cm^{-3}; D. Wang et al., 2014). The $N_{10–40nm}$ was comparable to 10–100 nm concentrations observed in various European cities (Németh et al., 2018), and slightly less than cities in North America (Jeong et al., 2010).

3.1.1. *Variability during COVID-19*

In early March 2020, Raleigh recorded its first COVID-19 case and executive orders pertaining to the pandemic began in the days following. Between March 10 and 17, 2020 North Carolina was under a state of emergency and all K-12 public schools, restaurants, and bars were mandated to close. After these executive orders, vehicular traffic on Western Blvd. decreased to approximately 1.4×10^4 vehicles per day (i.e., by ~ 67% of the average daily traffic) (Fig. S12). On March 23, gatherings of 50 or more people were banned, and service sector businesses were mandated to close. On March 30 the statewide stay at home order began. During the stay at home order, local traffic counts were reduced by ~75% of the average daily traffic. Human movement to retail and recreation, grocery and pharmacy, transit stations, and the workplace were down approximately 50%, 28%, 77%, and 45%, respectively according to the Wake County community mobility report. As the stay at home order persisted into late April and early May, movement to parks increased from 5 to 47%. As shown in Fig. 3.2, monthly averaged $N_{5–10nm}$ decreased from ~900 cm^{-3} between November 15 and March 15 to ~400 cm^{-3} between March 15 to May 15. Similarly, monthly averaged $N_{10–40nm}$ decreased from ~4300 cm^{-3} (Nov. 15 to Mar. 15) to ~2900 cm^{-3} (Mar. 15 to May 15). The decrease in number concentration during the COVID-19 shutdown can be attributed to reduced rush hour traffic. Fig. 3 shows the diurnal profile of hourly averaged $N_{10–40nm}$ on days before and during the COVID-19 pandemic with low morning and evening PBLH. Days with low (<250 m) morning and evening PBLH were selected because Meskhidze et al. (2019) found that the effect of rush hour traffic on the concentration was only observed when morning and evening PBLH was below 250 m. According to Fig. 3 the midday $N_{10–40nm}$ during COVID-19 is greater than pre-COVID-19 because the outbreak period encompasses spring months with stronger solar radiation leading to greater daytime convective mixing, higher PBLH and hence more dilution of near-surface emissions. During low boundary layer height, characteristic peaks in number concentration are visible in the morning and evening, and these are associated with rush hour traffic (Meskhidze et al., 2019). Prior to COVID-19, the diurnal $N_{10–40nm}$ would nearly double during rush hour on days with low morning and evening PBLH. On days with a similar PBLH pattern during the shutdown, the concentration peaks due to rush hour traffic are not so pronounced, and the average $N_{10–40nm}$ remains around 5×10^3 cm^{-3}. However, during the shutdown, there is a noon-time peak in concentrations that was not previously measured. This is possibly due to greater flexibility in people's schedule to travel to grocery stores, parks, etc. during the day. The same variations were seen in the $N_{5–10nm}$ concentration during COVID-19; however, concentrations are much lower (<1.5×10^3 cm^{-3}) than the average $N_{5–10nm}$ concentration (Fig. S13). Recent studies in China and India observed 20–40% decreases in average $PM_{2.5}$ concentration during the pandemic (Sharma et al., 2020; P. Wang et al., 2020). Here, the $PM_{2.5}$ concentration also decreased during this period (Fig. S14), but the concentration generally remained within the statistical fluctuation of the last 10 years.

3.2. *New particle formation events*

New particle formation events occurred during nearly all months of measurement. Fig. 4 summarizes the frequency of NPF events between

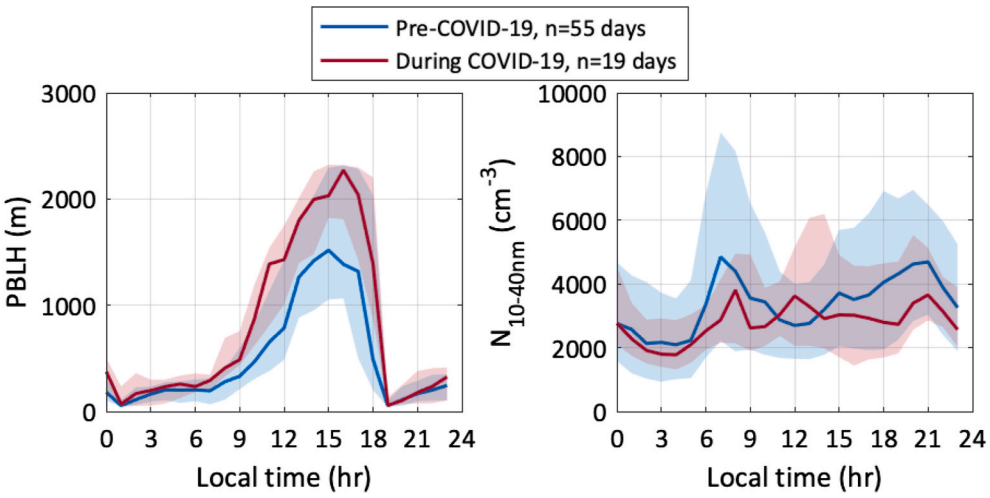

Fig. 3. Diurnal profiles of median planetary boundary layer height (PBLH, left) and number concentration of 10–40 nm particles (right). Colors correspond to time period before and after COVID-19 social distancing measures took effect. Shaded areas represent the 25th and 75th quartiles of the data. Pre-COVID-19 encompasses days from spring 2019 and winter/spring 2019/2020 prior to March 14, 2020. COVID-19 days include days between March 14, 2020 and May 15, 2020. (For interpretation of the references to colour in this figure legend, the reader is referred to the Web version of this article.)

the 15th day of each month. April/May 2020 had the highest frequency of events with 14 total events. Whereas, only two events were observed in May/June 2019. There were also no Class A events between April 15 and June 15, 2019. Many year-long measurement campaigns in North America found the highest NPF frequency to be during the spring (Pillai et al., 2013; Pryor et al., 2010; Stanier et al., 2004). In our measurements, Class C events were the most frequent, with approximately 3.6 events per month. Occurrence of Class A and B events were lower with 1.7 and 2.3 events per month, respectively. A study performed in Duke Forest, located ~39 km NW of our data collection site, also observed that Class C events were most frequent (Pillai et al., 2013).

The start time of NPF events varies greatly based on the class of event. The average start and detection times presented in Table 3 show that Class A NPF events were generally detected during the morning hours, while Class B events were detected during or after midday. The estimated average start time of all Class A events was 9:30 ± 01:00 and the average detection time was 11:00 ± 1:15. The average minimum and maximum start times reported in Table 3 represent the starting time range estimated based on one standard deviation of the 5–10 nm GR. All

Table 3
Average NPF event statistics for Class A and B events. All values reported are averages and the corresponding standard deviation of all events in each class. Estimated start time and detection time are rounded to the nearest 15 min interval.

NPF Event Type	Estimated Start Time	Detection Time	5–10 nm GR (nm hr^{-1})	10–20 nm GR (nm hr^{-1})	20–30 nm GR (nm hr^{-1})
Class A	9:30 ± 01:00	11:00 ± 1:15	2.3 ± 1.2	3.1 ± 2.2	2.6 ± 1.2
Class B		14:00 ± 4:30		3.7 ± 2.9	3.3 ± 2.3

Class A event times are detailed in Table S1. The general start time of all Class A events was also pronounced in the diurnal variation of particle number concentration plots shown in Fig. 5a. The average $N_{5–10nm}$ and $N_{10–40nm}$ increases first between 06:00 and 09:00 likely due to rush-hour traffic, and again between 09:00 and 12:00 correlating with the average detection time of the nucleated particles. The onset of a Class A NPF

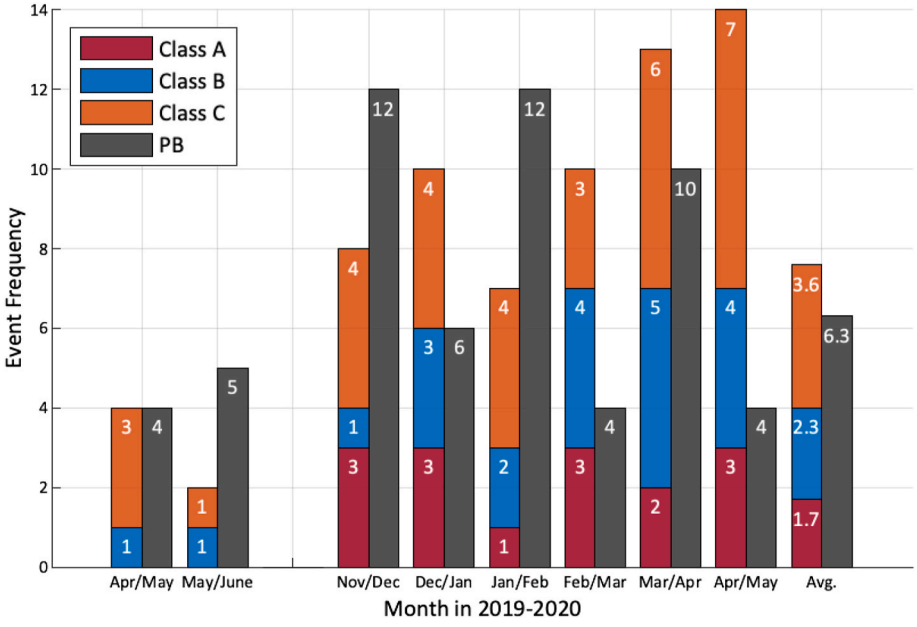

Fig. 4. Frequency of NPF and PB (black) events between the 15th day of each month during all measurement campaigns. NPF frequency bars are divided into Class A (red), B (blue), C (orange). (For interpretation of the references to colour in this figure legend, the reader is referred to the Web version of this article.)

event increases the $N_{5–10nm}$ by almost a factor of two compared to the concentration on a non-NPF day (see Fig. 5b). The morning traffic signature was also present in the $N_{10–40nm}$ diurnal variation. Fig. 5a shows that the concentration increase due to NPF was delayed on average by ~60 min from the onset of the $N_{5–10nm}$, as the particles grow into the larger size range. In Duke Forest, the average onset for all NPF events occurred between 06:00–07:00 during the spring and summer while winter events occurred later in the day around 14:00 (Pillai et al., 2013). The average detection time for Class B NPF events was 14:00 ± 4:30, with the earliest detected at 07:00 on December 31, 2019 and three nighttime NPF events detected at 23:30 on March 13 and 20, 2020, and 22:45 on April 21, 2020. The variability in Class B event detection times caused no significant diurnal pattern in the particle number concentration on Class B days (see Table S2 and Fig. S15).

The particle GRs were broken down into three different size ranges (5–10 nm, 10–20 nm, and 20–30 nm) to analyze how particle growth varies with modal size. Little variation was observed between size ranges in the Class A GRs (5–10 nm: 2.3 ± 1.2 nm h^{-1}; 10–20 nm: 3.1 ± 2.2 nm h^{-1}; 20–30 nm: 2.6 ± 1.2 nm h^{-1}). Particle growth rates during Class B events were slightly greater than Class A events. The average GRs were 3.7 ± 2.9 and 3.3 ± 2.3 nm h^{-1} for 10–20 nm and 20–30 nm, respectively. The Class B GR values measured during this study were comparable to rates previously measured on the NCSU campus (10–25 nm GR: 1.6–3.9 nm h^{-1}; 26–40 nm GR: 2.7–5.7 nm h^{-1}; Meskhidze et al., 2019). The 5–10 nm Class A GRs recorded in Raleigh were less than urban GRs in Hong Kong (3.7–8.3 nm h^{-1}; D. Wang et al., 2014) between 5.5 and 10 nm. The Class A and B 10–20 nm GR were less than the average 7–20 nm GR measured in Hyytiälä, Finland (4.3 nm h^{-1}; Yli-Juuti et al., 2011) and Shanghai, China (11.4 nm h^{-1}; Xiao et al., 2015). All studies chosen for GR comparison were selected because the size ranges of the reported GRs most closely matched the ranges analyzed in this work (5–10 nm, 10–20 nm, and 20–30 nm).

Analysis of meteorological variables and criteria pollutants during Class A and B NPF days revealed unique conditions for NPF events (Figs. S16 and S17). Class A and B NPF events occur on days with intense solar radiation with the noontime values exceeding 600 W m^{-2}. High actinic flux and low wind speeds caused enhanced vertical turbulence and expansion of the PBLH above 2000 m during midday. Relative humidity was lower on Class A and B days (30–60%) than on regular days (40–90%). Comparable solar radiation and relative humidity conditions have been reported for NPF events in other locations around the world (Boy and Kulmala, 2002; Jaatinen et al., 2009; Sihto et al., 2006). Class A event days were characterized by elevated O_3 concentrations (most likely caused by high actinic flux) and low $PM_{2.5}$ compared to non-event days. O_3 concentrations were also elevated during Class B event days; however, $PM_{2.5}$ levels were comparable to non-event days.

3.3. Particle burst events

Particle burst events play a significant role in shaping the near-surface particle concentration and size distribution in Raleigh. These bursts of sub-10 nm particles were observed during all hours of the day and their duration lasted anywhere between 7 and 93 h. Fig. 4 (and Figs. S3 and S4) show that these events occurred during all months, with an average of 6 PB event days per month. The month-long periods between November 15 and December 15, 2019; and January 15 and February 15, 2020 had the greatest frequency of PB days with events spanning a total of 13 days. The lowest frequency of events was only 4 days during April/May 2019 and 2020, and February/March 2020.

The PB events observed were characterized by a factor of two increase in $N_{5–10nm}$ due to continuous bursts of sub-10 nm particles (example event shown in Fig. S18). However, when compared to a regular day, there was no change in the $N_{10–40nm}$ (Fig. 5c). The average $N_{5–10nm}$ during all events ranged between 7.7×10^3–6.9×10^4 cm^{-3}. No modal growth of the particles was measured during PB events, suggesting that the particles were produced by an isolated source. The average mode diameter of all PBs was between 5 and 7.5 nm suggesting that particles had a limited time to grow (i.e., the source was in the vicinity of the measurement site). Occasionally, the mode diameter would drop below 5 nm causing the $N_{5–10nm}$ to peak over 5×10^4 cm^{-3}. No change in the average $N_{10–40nm}$ concentration and little deviation in the modal diameter confirms that no modal growth was measured during these events. Concentrations measured during the strongest PB events were greater than the maximum nucleation mode concentrations observed in Hong Kong (1.9×10^4 cm^{-3}; D. Wang et al., 2014), and less than those observed in Brisbane (10×10^4 cm^{-3}; Cheung et al., 2011). The observed mean diameters were less than those observed during PB events in China (24 nm; D. Wang et al., 2014), Australia (14 nm; Cheung et al., 2011), and Korea (25 nm; Park et al., 2008).

On three measurement days (Jan. 17 and 21; and Feb. 21, 2020) a Class B NPF event and a PB event were detected simultaneously (Fig. S19). As newly nucleated particles grew characteristically of an NPF event, the pre-existing PB sub-10 nm particles persisted throughout the growth event maintaining a constant mode diameter. The decoupled nature of these two events also suggests that the PB particles likely originated from a local source and had similar sizes when reached the detection instrument. Fig. S19 also shows that there was little coagulation between the particles produced by two distinct sources, i.e., ones produced by a mesoscale NPF event and by a local source. The large spatial extent of the NPF event allowed for particles to grow as they advected toward the measurement instrument. Providing that the direct measurement of the local pollutant persisted, detection of the PB event particles continued throughout the growth event. The PB event particles

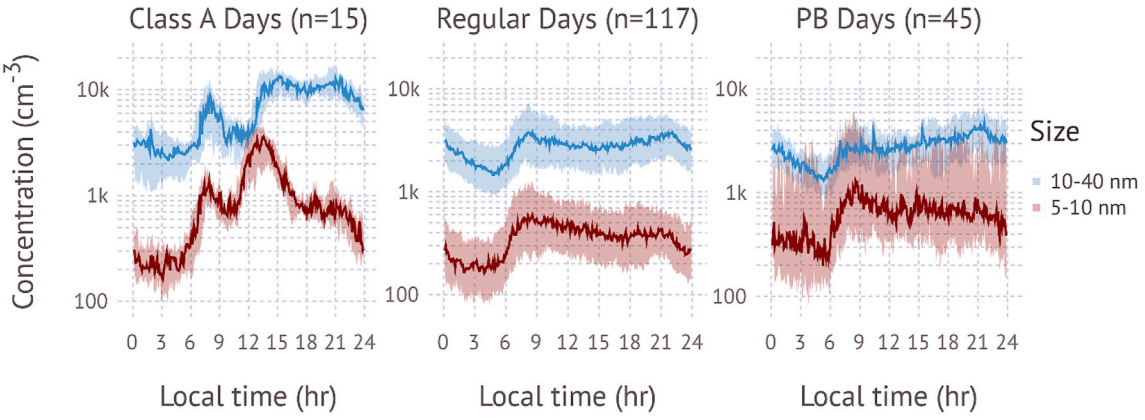

Fig. 5. Diurnal trend for Class A NPF days, regular days, and PB days. Data correspond to 5 min time average integrated SMPS concentration for 5–10 and 10–40 nm size range. Solid lines are the median concentration. Shades are the interquartile range. (For interpretation of the references to colour in this figure legend, the reader is referred to the Web version of this article.)

likely contributed to the growth event, albeit without measurable modal growth.

Wind analysis on PB days shown in Fig. 6 reveals that the wind was blowing from the NNE and NE 40% of the of time. Whereas, the winds out of the SSW were most frequent on regular days. On PB days, the highest average $N_{5–10nm}$ were measured during NE winds and exceeded 2×10^4 cm^{-3}. Subtle peaks in S and E winds also correlated with average $N_{5–10nm}$ concentrations greater than 1×10^4 cm^{-3}. Some PB events occurred during overcast weather and periods of rainfall, which had no impact on removal of the sub-10 nm particles (Table S3). Additionally, both the PBLH and solar radiation remained lower on PB days compared to regular days (Fig. S16). Low PBLH, solar radiation, and the strong correlation with NE winds on PB days suggests that aerosol dispersion processes were weak, allowing for direct measurements of a pollution plume created by a local source. Studies that also observed PB events suggest weak aerosol dispersion processes allowed for measurement of pollutants emitted from local combustion sources such as power plants (Gao et al., 2009), airports (Cheung et al., 2011), and funeral homes (D. Wang et al., 2014). In contrast, Park et al. (2008) attributed their burst events to photochemical nucleation of particles.

3.4. Sources of sub-10 nm particles

The frequent observance of PB events suggests the presence of large sources directly emitting sub-10 nm particles in Raleigh. Fig. 7a shows multiple locations in and around Raleigh where the ambient concentrations of 2.5–11 nm particles exceeded 1×10^5 cm^{-3} (and Figs. S8 and S9). One likely source of particles was the RDU International Airport located in NW Raleigh. During the three deployments in March 2020, the sub-10 nm particle number concentration within and around the terminal of the airport exceeded 1×10^5 cm^{-3}. UFP number concentrations of this magnitude were also recorded at airports worldwide (Brilke et al., 2020; Hudda et al., 2014; Keuken et al., 2012; Ren et al., 2016; Zhu et al., 2011). The nucleation mode was the most prominent in the airport size distributions with modal diameters of 12 nm (Westerdahl et al., 2008), and 14 nm (Zhu et al., 2011) near Los Angeles International Airport, 16 nm at Tianjin International Airport (Ren et al., 2016), and 12.6 nm at the Paphos Airport (Brilke et al., 2020). Fig. 7a (and Figs. S8 and S9) show that aside from the airport, there were few other isolated high-concentration locations throughout the March mobile deployments.

Mobile deployments 4–6 (shown in Figs. 7b, S10, and S11) highlight a multitude of sub-10 nm particle sources closer to the measurement site on campus and one further south. Two significant sources producing $N_{2.5–11nm}$ concentrations greater than 2×10^4 cm^{-3} are located to the NE and SE of Jordan Hall. These spots of elevated concentration correspond to the locations of the NCSU campus utility plants. The Cates Ave. Utility Plant and Yarbrough Boiler located to the NE of Jordan Hall and the Centennial Campus Plant is to the south. Peaks in the number concentration greater than 2×10^4 cm^{-3} on PB event days also correlate with winds from the NE and SSE. It is likely that the PB event particles measured by the SMPS system at Jordan Hall were produced from the Cates Ave. Utility Plant and Yarbrough Dr. Boiler. Consistent NE winds and weak aerosol dispersion processes allow for the continuous collection of the plume originating from this plant. The weak peak in number concentration correlating with SSE winds was also likely caused by plumes generated at the Centennial Campus Utility Plant. Gao et al. (2009) concluded that the PB events measured during their study resulted from local power plant plumes. On-site measurements at natural gas burning plants observed 2–7 nm sized particles in concentrations ranging from 1.27×10^5 to 1.7×10^7 cm^{-3} (Bond et al., 2006; Brewer et al., 2016; Shi et al., 2001).

The multitude of concentration hotspots observed during the mobile deployments suggests there are many point sources in Raleigh directly emitting large numbers of particles that contribute significantly to the local particle number concentration. Previous studies have suggested that excessive emissions can occur when driving a vehicle on grades (Cicero-Fernández et al., 1997). To check if the observed hotspots in particle concentration were associated with road hills, the spatial concentration maps were compared against elevation maps (Figs. S20 and

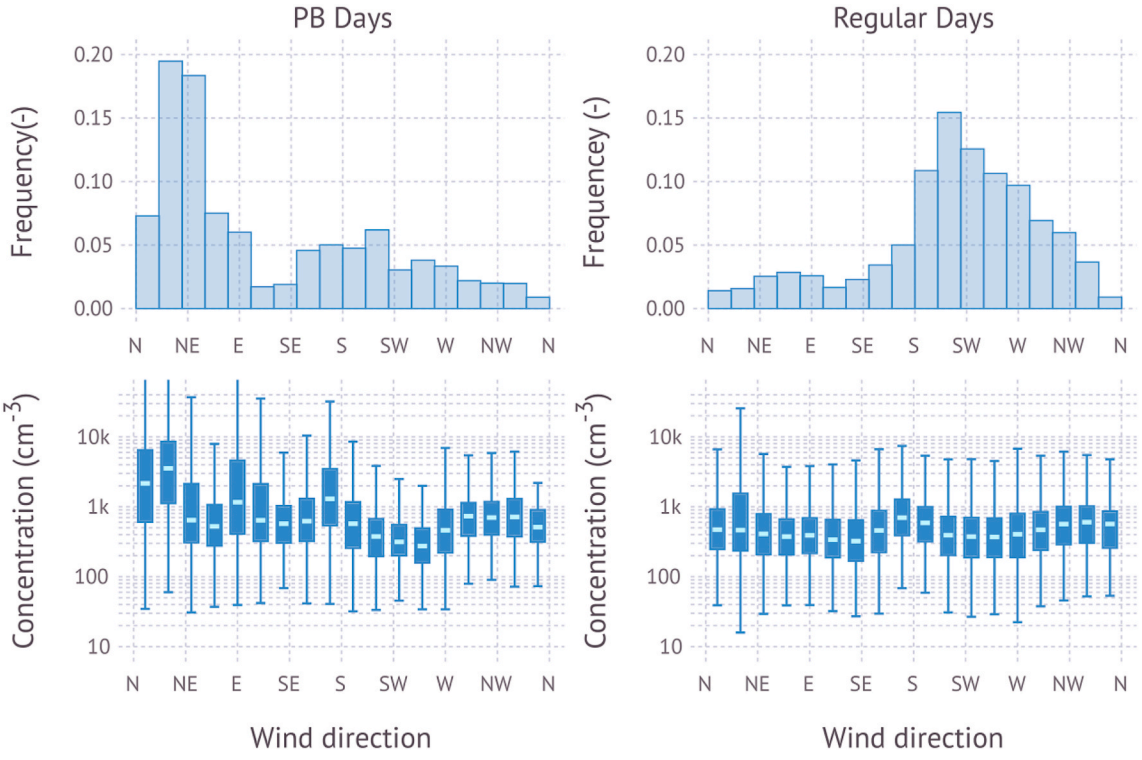

Fig. 6. Top plots show the frequency distribution of observed wind direction. Bottom plots show box-and-whisker plots of the number concentration of 2.5–10 nm particles. Left: PB event days, right: regular days.

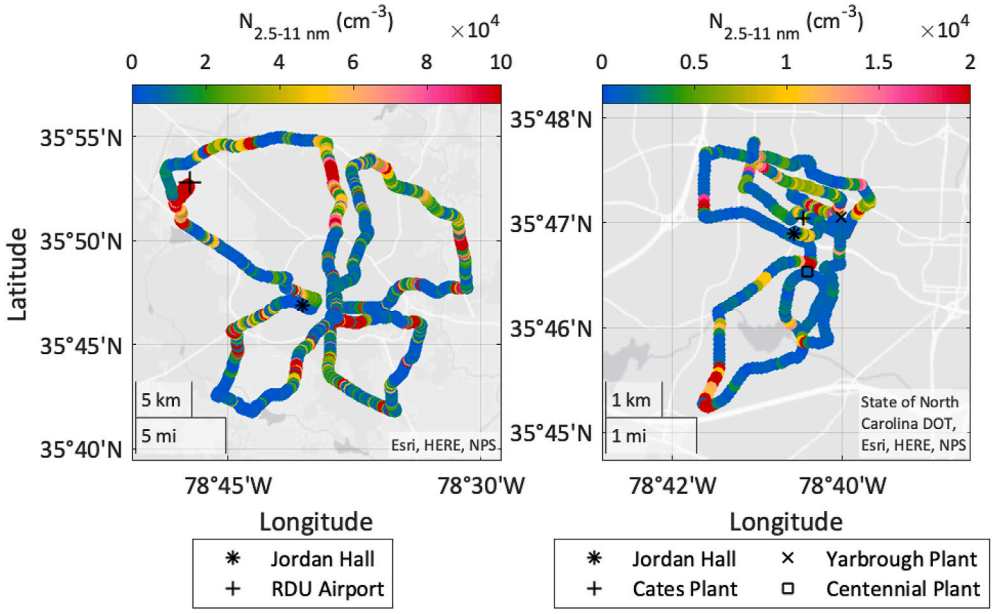

Fig. 7. Spatial distribution of the number concentration of 2.5–11 nm size particles derived from the mobile deployments. Left: Mobile deployment 3 on March 23, 2020 covering the Raleigh metropolitan area including the Raleigh-Durham Airport (RDU). Right: Mobile deployment 4 on April 29, 2020 covering NCSU campus and areas surrounding the Jordan Hall measurement site. Also indicated are the locations of the NCSU utility plants (Cates, Yarborough, and Centennial).

S21). No relationship was found between the isolated high particle concentrations and changes in elevation, suggesting that vehicular emissions associated with changing driving conditions do not likely contribute to the observed concentration hotspots in Raleigh, NC. During the mobile deployments, 2.5–11/10 nm sized particles accounted for ~45–71% of the total number concentration greater than 2.5 nm depending on the drive. A similar study in Birmingham, UK found that the 3–7 nm particles produced from the local utility plant accounted for 53% of the UFP number concentration (Shi et al., 2001). Over the extended time, the sub-10 nm particles can both grow into large sizes to act as cloud condensation nuclei and aid in particle growth through coagulation (Merikanto et al., 2009; D. L. Yue et al., 2011).

Although multiple sources of sub-40 nm particles were identified, there are likely potential sources of UFPs that are greater than 40 nm in size and were not analyzed in this study. Particles resulting from biomass and biofuel combustion have mode diameters between 30 and 123 nm in diameter and can also contribute to cloud condensation nuclei concentrations (Allouis et al., 2010; Posner and Pandis, 2015; Rissler et al., 2006; Tan et al., 2009). In future measurements, the use of an SMPS system with an extended size range would allow for a broader understanding of UFP sources contributing to Raleigh's size distribution.

4. Conclusions

Ambient aerosol size distribution measurements in Raleigh, NC from April to June 2019, and November 2019 to May 2020 show great variability in sub-40 nm concentrations due to NPF and PB events. During the 231 measurement days, 15 and 21 Class A and B NPF events occurred. Class A events were most common during the late-morning with an average detection time of 11:00 ± 1:15, while Class B events began later in the day around 14:00 ± 4:30. NPF events were most favorable on days with elevated solar radiation resulting in a high diurnal PBLH, and low relatively humidity. Class B GRs in all size ranges were greater than Class A. 28 PB events of 5–7.5 nm sized particles with average $N_{5–10nm}$ concentrations of 7.7×10^3–6.9×10^4 cm^{-3} were also observed throughout all measurement campaigns. The continual bursts of particles lasted between 7 and 93 h and occurred primarily during NE winds. A secondary, weak increase in concentration also correlated with S winds. Low solar radiation, surface wind speed, and PBLH suggest weak aerosol dispersion processes allowing for continual measurement of a local pollutant plume. Mobile deployments throughout the NCSU campus revealed that the campus utility plants were likely the significant sources of sub-10 nm particles measured during PB events. Mobile sub-10 nm particle number concentrations near these facilities ranged up to 2×10^4 cm^{-3}. The RDU international airport was also identified as a consist source of sub-10 nm particles with number concentrations exceeding 1×10^5 cm^{-3}. Further stationary on-site and near-by ambient measurements at the airport, utility plants, and other industrial activities associated with the release of sub-10 nm sized particles into the atmosphere would provide a better understanding of the contributions of point sources of particles on Raleigh's urban aerosol number budget and size distribution.

Data availability

Supplementary information is available in the online version of this paper. Data acquisition software used to collect the data, raw data reported by the instruments, processed data, and scripts to generate the figures are accessible through zenodo.org (http://doi.org/10.5281/zenodo.3958098).

CRediT authorship contribution statement

Alyssa Zimmerman: Investigation, Formal analysis, Visualization, Writing - original draft, Data curation. **Markus D. Petters:** Funding acquisition, Conceptualization, Supervision, Software, Validation, Formal analysis, Visualization, Data curation, Writing - review & editing. **Nicholas Meskhidze:** Funding acquisition, Conceptualization, Supervision, Validation, Writing - review & editing.

Declaration of competing interest

The authors declare that they have no known competing financial interests or personal relationships that could have appeared to influence the work reported in this paper.

Acknowledgements

This work was funded by grant NSF-AGS 1946340. We gratefully acknowledge Jason Weinstein from the U.S. Environmental Protection Agency for lending us the TSI 3776c condensation particle counter. The funding agency is the U.S. National Science Foundation (NSF) under grant NSF-AGS 1946340.

Appendix A. Supplementary data

Supplementary data to this article can be found online at https://doi.org/10.1016/j.atmosenv.2020.117835.

References

Agus, E.L., Lingard, J.J.N., Tomlin, A.S., 2008. Suppression of nucleation mode particles by biomass burning in an urban environment: a case study. J. Environ. Monit. 10 (8), 979. https://doi.org/10.1039/b803871f.

Alanen, J., Saukko, E., Lehtoranta, K., Murtonen, T., Timonen, H., Hillamo, R., et al., 2015. The formation and physical properties of the particle emissions from a natural gas engine. Fuel 162, 155–161. https://doi.org/10.1016/j.fuel.2015.09.003.

Alföldy, B., Giechaskiel, B., Hofmann, W., Drossinos, Y., 2009. Size-distribution dependent lung deposition of diesel exhaust particles. J. Aerosol Sci. 40 (8), 652–663. https://doi.org/10.1016/j.jaerosci.2009.04.009.

Allouis, C., Beretta, F., Minutolo, P., Pagliara, R., Sirignano, M., Sgro, L.A., D'Anna, A., 2010. Measurements of ultrafine particles from a gas-turbine burning biofuels. Exp. Therm. Fluid Sci. 34 (3), 258–261. https://doi.org/10.1016/j.expthermflusci.2009.10.034.

Asgharian, B., Price, O.T., 2007. Deposition of ultrafine (NANO) particles in the human lung. Inhal. Toxicol. 19 (13), 1045–1054. https://doi.org/10.1080/08958370701626501.

Baranizadeh, E., Arola, A., Hamed, A., Nieminen, T., Mikkonen, S., Virtanen, A., et al., 2014. The effect of cloudiness on new-particle formation: investigation of radiation levels. Boreal Environ. Res. 19, 343–354.

Bianchi, F., Trostl, J., Junninen, H., Frege, C., Henne, S., Hoyle, C.R., et al., 2016. New particle formation in the free troposphere: a question of chemistry and timing. Science 352 (6289), 1109–1112. https://doi.org/10.1126/science.aad5456.

Bond, T.C., Wehner, B., Plewka, A., Wiedensohler, A., Heintzenberg, J., Charlson, R.J., 2006. Climate-relevant properties of primary particulate emissions from oil and natural gas combustion. Atmos. Environ. 40 (19), 3574–3587. https://doi.org/10.1016/j.atmosenv.2005.12.030.

Bousiotis, D., Dall'Osto, M., Beddows, D.C.S., Pope, F.D., Harrison, R.M., 2019. Analysis of new particle formation (NPF) events at nearby rural, urban background and urban roadside sites. Atmos. Chem. Phys. 19 (8), 5679–5694. https://doi.org/10.5194/acp-19-5679-2019.

Boy, M., Kulmala, M., 2002. Nucleation events in the continental boundary layer: influence of physical and meteorological parameters. Atmos. Chem. Phys. 2 (1), 1–16. https://doi.org/10.5194/acp-2-1-2002.

Boy, M., Karl, T., Turnipseed, A., Mauldin, R.L., Kosciuch, E., Greenberg, J., et al., 2008. New particle formation in the front range of the Colorado rocky mountains. Atmos. Chem. Phys. 8 (6), 1577–1590. https://doi.org/10.5194/acp-8-1577-2008.

Brewer, E., Li, Y., Finken, B., Quartucy, G., Muzio, L., Baez, A., et al., 2016. PM2.5 and ultrafine particulate matter emissions from natural gas-fired turbine for power generation. Atmos. Environ. 131, 141–149. https://doi.org/10.1016/j.atmosenv.2015.11.048.

Brilke, S., Fölker, N., Müller, T., Kandler, K., Gong, X., Peischl, J., et al., 2020. New particle formation and sub-10 nm size distribution measurements during the A-LIFE field experiment in Paphos, Cyprus. Atmos. Chem. Phys. 20 (9), 5645–5656. https://doi.org/10.5194/acp-20-5645-2020.

Cheung, H.C., Morawska, L., Ristovski, Z.D., 2011. Observation of new particle formation in subtropical urban environment. Atmos. Chem. Phys. 11 (8), 3823–3833. https://doi.org/10.5194/acp-11-3823-2011.

Cicero-Fernândez, P., Long, J.R., Winer, A.M., 1997. Effects of grades and other loads on on-road emissions of hydrocarbons and carbon monoxide. J. Air Waste Manag. Assoc. 47 (8), 898–904. https://doi.org/10.1080/10473289.1997.10464455.

Collins, A.M., Dick, W.D., Romay, F.J., 2013. A new coincidence correction method for condensation particle counters. Aerosol. Sci. Technol. 47 (2), 177–182. https://doi.org/10.1080/02786826.2012.737049.

Dal Maso, M., 2002. Condensation and coagulation sinks and formation of nucleation mode particles in coastal and boreal forest boundary layers. J. Geophys. Res. 107 (D19), 8097. https://doi.org/10.1029/2001JD001053.

Dal Maso, M., Kulmala, M., Riipinen, I., Wagner, R., Hussein, T., Aalto, P.P., Lehtinen, K. E.J., 2005. Formation and growth of fresh atmospheric aerosols: eight years of aerosol size distribution data from SMEAR II, Hyytiälä, Finland. Boreal Environ. Res. 10, 323–336.

Gao, J., Wang, T., Zhou, X., Wu, W., Wang, W., 2009. Measurement of aerosol number size distributions in the Yangtze River delta in China: formation and growth of particles under polluted conditions. Atmos. Environ. 43 (4), 829–836. https://doi.org/10.1016/j.atmosenv.2008.10.046.

Größ, J., Hamed, A., Sonntag, A., Spindler, G., Manninen, H.E., Nieminen, T., et al., 2018. Atmospheric new particle formation at the research station Melpitz, Germany: connection with gaseous precursors and meteorological parameters. Atmos. Chem. Phys. 18 (3), 1835–1861. https://doi.org/10.5194/acp-18-1835-2018.

Harrison, R.M., Grenfell, J.L., Savage, N., Allen, A., Clemitshaw, K., Penkett, S., et al., 2000. Observations of new particle production in the atmosphere of a moderately polluted site in eastern England. J. Geophys. Res.: Atmosphere 105 (D14), 17819–17832. https://doi.org/10.1029/2000JD900086.

Hudda, N., Gould, T., Hartin, K., Larson, T.V., Fruin, S.A., 2014. Emissions from an international airport increase particle number concentrations 4-fold at 10 km downwind. Environ. Sci. Technol. 48 (12), 6628–6635. https://doi.org/10.1021/es5001566.

Hussein, Atashi, Sogacheva, Hakala, Dada, Petäjä, Kulmala, 2020. Characterization of urban new particle formation in amman—Jordan. Atmosphere 11 (1), 79. https://doi.org/10.3390/atmos11010079.

Jaatinen, A., Hamed, A., Joutsensaari, J., Mikkonen, S., Birmili, W., Wehner, B., et al., 2009. A comparison of new particle formation events in the boundary layer at three different sites in Europe. Boreal Environ. Res. 14, 481–498.

Jeong, C.-H., Evans, G.J., McGuire, M.L., Chang, R.Y.-W., Abbatt, J.P.D., Zeromskiene, K., et al., 2010. Particle formation and growth at five rural and urban sites. Atmos. Chem. Phys. 10 (16), 7979–7995. https://doi.org/10.5194/acp-10-7979-2010.

Kalkavouras, P., Bougiatioti, A., Grivas, G., Stavroulas, I., Kalivitis, N., Liakakou, E., et al., 2020. On the regional aspects of new particle formation in the Eastern Mediterranean: a comparative study between a background and an urban site based on long term observations. Atmos. Res. 239, 104911 https://doi.org/10.1016/j.atmosres.2020.104911.

Karl, M., Kukkonen, J., Keuken, M.P., Lützenkirchen, S., Pirjola, L., Hussein, T., 2016. Modeling and measurements of urban aerosol processes on the neighborhood scale in Rotterdam, Oslo and Helsinki. Atmos. Chem. Phys. 16 (8), 4817–4835. https://doi.org/10.5194/acp-16-4817-2016.

Kerminen, V.-M., Chen, X., Vakkari, V., Petäjä, T., Kulmala, M., Bianchi, F., 2018. Atmospheric new particle formation and growth: review of field observations. Environ. Res. Lett. 13 (10), 103003 https://doi.org/10.1088/1748-9326/aadf3c.

Keuken, M.P., Henzing, J.S., Zandveld, P., van den Elshout, S., Karl, M., 2012. Dispersion of particle numbers and elemental carbon from road traffic, a harbour and an airstrip in The Netherlands. Atmos. Environ. 54, 320–327. https://doi.org/10.1016/j.atmosenv.2012.01.012.

Kulmala, M., 2003. Atmospheric science: how particles nucleate and grow. Science 302 (5647), 1000–1001. https://doi.org/10.1126/science.1090848.

Kulmala, Markku, Petäjä, T., Nieminen, T., Sipilä, M., Manninen, H.E., Lehtipalo, K., et al., 2012. Measurement of the nucleation of atmospheric aerosol particles. Nat. Protoc. 7 (9), 1651–1667. https://doi.org/10.1038/nprot.2012.091.

Li, N., Sioutas, C., Cho, A., Schmitz, D., Misra, C., Sempf, J., et al., 2003. Ultrafine particulate pollutants induce oxidative stress and mitochondrial damage. Environ. Health Perspect. 111 (4), 455–460. https://doi.org/10.1289/ehp.6000.

Mäkelä, J.M., Maso, M.D., Pirjola, L., Keronen, P., Laakso, L., Kulmala, M., Laaksonen, A., 2000. Characteristics of the atmospheric particle formation events observed at a borel forest site in southern Finland. Boreal Environ. Res. 5, 299–313.

Malorni, L., Guida, V., Sirignano, M., Genovese, G., Petrarca, C., Pedata, P., 2017. Exposure to sub-10 nm particles emitted from a biodiesel-fueled diesel engine: in vitro toxicity and inflammatory potential. Toxicol. Lett. 270, 51–61. https://doi.org/10.1016/j.toxlet.2017.02.009.

Merikanto, J., Spracklen, D.V., Mann, G.W., Pickering, S.J., Carslaw, K.S., 2009. Impact of nucleation on global CCN. Atmos. Chem. Phys. 9 (21), 8601–8616. https://doi.org/10.5194/acp-9-8601-2009.

Meskhidze, N., Jaimes-Correa, J.C., Petters, M.D., Royalty, T.M., Phillips, B.N., Zimmerman, A., Reed, R., 2019. Possible wintertime sources of fine particles in an urban environment. J. Geophys. Res.: Atmosphere 124 (23), 13055–13070. https://doi.org/10.1029/2019JD031367.

Minutolo, P., D'Anna, A., Commodo, M., Pagliara, R., Toniato, G., Accordini, C., 2008. Emission of ultrafine particles from natural gas domestic burners. Environ. Eng. Sci. 25 (10), 1357–1364. https://doi.org/10.1089/ees.2007.0188.

Mirme, S., Mirme, A., Minikin, A., Petzold, A., Horrak, U., 2010. Atmospheric sub-3 nm particles at high altitudes. Atmos. Chem. Phys. 10, 437–451. https://doi.org/10.5194/acp-10-437-2010.

Morawska, L., Ristovski, Z., Jayaratne, E.R., Keogh, D.U., Ling, X., 2008. Ambient nano and ultrafine particles from motor vehicle emissions: characteristics, ambient processing and implications on human exposure. Atmos. Environ. 42 (35), 8113–8138. https://doi.org/10.1016/j.atmosenv.2008.07.050.

Myhre, G., Shindell, D., Bréon, F.-M., Collins, W., Fuglestvedt, J., Huang, J., et al., 2013. 8 Anthropogenic and Natural Radiative Forcing. Cambridge University Press, USA. Cambridge, United Kingdom and New York, NY.

Németh, Z., Rosati, B., Zíková, N., Salma, I., Bozó, L., Dameto de España, C., et al., 2018. Comparison of atmospheric new particle formation events in three Central European cities. Atmos. Environ. 178, 191–197. https://doi.org/10.1016/j.atmosenv.2018.01.035.

Nieminen, T., Kerminen, V.-M., Petäjä, T., Aalto, P.P., Arshinov, M., Asmi, E., et al., 2018. Global analysis of continental boundary layer new particle formation based on long-term measurements. Atmos. Chem. Phys. 18 (19), 14737–14756. https://doi.org/10.5194/acp-18-14737-2018.

Nilsson, E.D., Rannik, U., Kulmala, M., Buzorius, G., O'Dowd, C.D., 2001. Effects of continental boundary layer evolution, convection, turbulence and entrainment, on aerosol formation. Tellus B 53 (4), 441–461. https://doi.org/10.1034/j.1600-0889.2001.530409.x.

Oberdörster, G., Sharp, Z., Atudorei, V., Elder, A., Gelein, R., Kreyling, W., Cox, C., 2004. Translocation of inhaled ultrafine particles to the brain. Inhal. Toxicol. 16 (6–7), 437–445. https://doi.org/10.1080/08958370490439597.

O'Dowd, C., McFiggans, G., Creasey, D.J., Pirjola, L., Hoell, C., Smith, M.H., et al., 1999. On the photochemical production of new particles in the coastal boundary layer. Geophys. Res. Lett. 26 (12), 1707–1710. https://doi.org/10.1029/1999GL900335.

Park, K., Park, J.Y., Kwak, J.-H., Cho, G.N., Kim, J.-S., 2008. Seasonal and diurnal variations of ultrafine particle concentration in urban Gwangju, Korea: observation of ultrafine particle events. Atmos. Environ. 42 (4), 788–799. https://doi.org/10.1016/j.atmosenv.2007.09.068.

Peters, A., Wichmann, H.E., Tuch, T., Heinrich, J., Heyder, J., 1997. Respiratory effects are associated with the number of ultrafine particles. Am. J. Respir. Crit. Care Med. 155 (4), 1376–1383. https://doi.org/10.1164/ajrccm.155.4.9105082.

Petters, M.D., 2018. A language to simplify computation of differential mobility analyzer response functions. Aerosol. Sci. Technol. 52 (12), 1437–1451. https://doi.org/10.1080/02786826.2018.1530724.

Pillai, P., Khlystov, A., Walker, J., Aneja, V., 2013. Observation and analysis of particle nucleation at a forest site in southeastern US. Atmosphere 4 (2), 72–93. https://doi.org/10.3390/atmos4020072.

Platis, A., Altstädter, B., Wehner, B., Wildmann, N., Lampert, A., Hermann, M., et al., 2016. An observational case study on the influence of atmospheric boundary-layer dynamics on new particle formation. Boundary-Layer Meteorol. 158 (1), 67–92. https://doi.org/10.1007/s10546-015-0084-y.

Posner, L.N., Pandis, S.N., 2015. Sources of ultrafine particles in the Eastern United States. Atmos. Environ. 111, 103–112. https://doi.org/10.1016/j.atmosenv.2015.03.033.

Pryor, S.C., Spaulding, A.M., Barthelmie, R.J., 2010. New particle formation in the Midwestern USA: event characteristics, meteorological context and vertical profiles. Atmos. Environ. 44 (35), 4413–4425. https://doi.org/10.1016/j.atmosenv.2010.07.045.

Pryor, S.C., Barthelmie, R.J., Sørensen, L.L., McGrath, J.G., Hopke, P., Petäjä, T., 2011. Spatial and vertical extent of nucleation events in the Midwestern USA: insights from the Nucleation in ForesTs (NIFTy) experiment. Atmos. Chem. Phys. 11 (4), 1641–1657. https://doi.org/10.5194/acp-11-1641-2011.

Ren, J., Liu, J., Li, F., Cao, X., Ren, S., Xu, B., Zhu, Y., 2016. A study of ambient fine particles at Tianjin International Airport, China. Sci. Total Environ. 556, 126–135. https://doi.org/10.1016/j.scitotenv.2016.02.186.

Rissler, J., Vestin, A., Swietlicki, E., Fisch, G., Zhou, J., Artaxo, P., Andreae, M.O., 2006. Size distribution and hygroscopic properties of aerosol particles from dry-season biomass burning in Amazonia. Atmos. Chem. Phys. 22.

Rose, C., Sellegri, K., Velarde, F., Moreno, I., Ramonet, M., Weinhold, K., et al., 2015. Frequent nucleation events at the high altitude station of Chacaltaya (5240 m a.s.l.), Bolivia. Atmos. Environ. 102, 18–29. https://doi.org/10.1016/j.atmosenv.2014.11.015.

Salma, I., Németh, Z., Kerminen, V.-M., Aalto, P., Nieminen, T., Weidinger, T., et al., 2016. Regional effect on urban atmospheric nucleation. Atmos. Chem. Phys. 16 (14), 8715–8728. https://doi.org/10.5194/acp-16-8715-2016.

Schröder, F., Ström, J., 1997. Aircraft measurements of sub micrometer aerosol particles (> 7 nm) in the midlatitude free troposphere and tropopause region. Atmos. Res. 44 (3–4), 333–356. https://doi.org/10.1016/S0169-8095(96)00034-8.

Seinfeld, J.H., Pandis, S.N., 2006. Atmospheric Chemistry and Physics: from Air Pollution to Climate Change. John Wiley, New York.

Sharma, S., Zhang, M., Anshika, Gao, J., Zhang, H., Kota, S.H., 2020. Effect of restricted emissions during COVID-19 on air quality in India. Sci. Total Environ. 728, 138878 https://doi.org/10.1016/j.scitotenv.2020.138878.

Shi, J.P., Evans, D.E., Khan, A.A., Harrison, R.M., 2001. Sources and concentration of nanoparticles (<10nm diameter) in the urban atmosphere. Atmos. Environ. 35 (7), 1193–1202. https://doi.org/10.1016/S1352-2310(00)00418-0.

Sihto, S.-L., Kulmala, M., Kerminen, V.-M., Dal Maso, M., Petäjä, T., Riipinen, I., et al., 2006. Atmospheric sulphuric acid and aerosol formation: implications from atmospheric measurements for nucleation and early growth mechanisms. Atmos. Chem. Phys. 6 (12), 4079–4091. https://doi.org/10.5194/acp-6-4079-2006.

Stanier, C.O., Khlystov, A.Y., Pandis, S.N., 2004. Nucleation events during the pittsburgh air quality study: description and relation to key meteorological, gas phase, and aerosol parameters special issue of *aerosol Science and technology* on findings from the fine particulate matter supersites program. Aerosol. Sci. Technol. 38 (Suppl. 1), 253–264. https://doi.org/10.1080/02786820390229570.

Stratmann, F., Siebert, H., Spindler, G., Wehner, B., Althausen, D., Heintzenberg, J., et al., 2003. New-particle formation events in a continental boundary layer: first results from the SATURN experiment. Atmos. Chem. Phys. 15.

Tan, P., Hu, Z., Lou, D., Li, B., 2009. Particle number and size distribution from a diesel engine with jatropha biodiesel fuel. In: SAE 2009 Powertrains Fuels and Lubricants Meeting, pp. 1–2726. https://doi.org/10.4271/2009-01-2726. Presented at the.

Wang, D., Guo, H., Cheung, K., Gan, F., 2014. Observation of nucleation mode particle burst and new particle formation events at an urban site in Hong Kong. Atmos. Environ. 99, 196–205. https://doi.org/10.1016/j.atmosenv.2014.09.074.

Wang, P., Chen, K., Zhu, S., Wang, P., Zhang, H., 2020. Severe air pollution events not avoided by reduced anthropogenic activities during COVID-19 outbreak. Resour. Conserv. Recycl. 158, 104814 https://doi.org/10.1016/j.resconrec.2020.104814.

Wang, S.C., Flagan, R.C., 1990. Scanning electrical mobility spectrometer. Aerosol. Sci. Technol. 13 (2), 230–240. https://doi.org/10.1080/02786829008959441.

Wang, Z.B., Hu, M., Sun, J.Y., Wu, Z.J., Yue, D.L., Shen, X.J., et al., 2013. Characteristics of regional new particle formation in urban and regional background environments in the North China Plain. Atmos. Chem. Phys. 13 (24), 12495–12506. https://doi.org/10.5194/acp-13-12495-2013.

Wehner, B., Siebert, H., Stratmann, F., Tuch, T., Wiedensohler, A., PetäJä, T., et al., 2007. Horizontal homogeneity and vertical extent of new particle formation events. Tellus B 59 (3), 362–371. https://doi.org/10.1111/j.1600-0889.2007.00260.x.

Westerdahl, D., Fruin, S., Fine, P., Sioutas, C., 2008. The Los Angeles International Airport as a source of ultrafine particles and other pollutants to nearby communities. Atmos. Environ. 42 (13), 3143–3155. https://doi.org/10.1016/j.atmosenv.2007.09.006.

Wichmann, H.-E., Peters, A., 2000. Epidemiological evidence of the effects of ultrafine particle exposure. Philos. Trans. R. Soc. London, Ser. A: Mathematical, Physical and Engineering Sciences 358 (1775), 2751–2769. https://doi.org/10.1098/rsta.2000.0682.

Willis, M.D., Burkart, J., Thomas, J.L., Köllner, F., Schneider, J., Bozem, H., et al., 2016. Growth of nucleation mode particles in the summertime Arctic: a case study. Atmos. Chem. Phys. 16 (12), 7663–7679. https://doi.org/10.5194/acp-16-7663-2016.

Xiao, S., Wang, M.Y., Yao, L., Kulmala, M., Zhou, B., Yang, X., et al., 2015. Strong atmospheric new particle formation in winter in urban Shanghai, China. Atmos. Chem. Phys. 15 (4), 1769–1781. https://doi.org/10.5194/acp-15-1769-2015.

Yli Juuti, T., Nieminen, T., Hirsikko, A., Aalto, P.P., Asmi, E., Hõrrak, U., et al., 2011. Growth rates of nucleation mode particles in Hyytiälä during 2003–2009: variation with particle size, season, data analysis method and ambient conditions. Atmospheric Chemistry and Physics 11 (24), 12865–12886. https://doi.org/10.5194/acp-11-12865-2011.

Yue, D., Hu, M., Wu, Z., Wang, Z., Guo, S., Wehner, B., et al., 2009. Characteristics of aerosol size distributions and new particle formation in the summer in Beijing. J. Geophys. Res. 114, D00G12 https://doi.org/10.1029/2008JD010894.

Yue, D.L., Hu, M., Zhang, R.Y., Wu, Z.J., Su, H., Wang, Z.B., et al., 2011. Potential contribution of new particle formation to cloud condensation nuclei in Beijing. Atmos. Environ. 45 (33), 6070–6077. https://doi.org/10.1016/j.atmosenv.2011.07.037.

Yue, D.L., Hu, M., Wang, Z.B., Wen, M.T., Guo, S., Zhong, L.J., et al., 2013. Comparison of particle number size distributions and new particle formation between the urban and rural sites in the PRD region, China. Atmos. Environ. 76, 181–188. https://doi.org/10.1016/j.atmosenv.2012.11.018.

Zhang, K.M., Wexler, A.S., 2002. A hypothesis for growth of fresh atmospheric nuclei. J. Geophys. Res.: Atmosphere 107 (D21). https://doi.org/10.1029/2002JD002180. AAC 15-1-AAC 15-6.

Zhu, Y., Fanning, E., Yu, R.C., Zhang, Q., Froines, J.R., 2011. Aircraft emissions and local air quality impacts from takeoff activities at a large International Airport. Atmos. Environ. 45 (36), 6526–6533. https://doi.org/10.1016/j.atmosenv.2011.08.062.